



Journal of Renewable Energies

Revue des Energies Renouvelables

journal home page : <https://revue.cder.dz/index.php/rer>

Research Paper

Experimental and CFD investigation of cavitation phenomenon in the distributor of a Banki-Michell Turbine

Jean Bosco Niyonzima ^{a,*}, Patrick Hendrick ^b

^a Université du Burundi, Centre de Recherche en Infrastructures, Environnement et technologie (CRIET), Chaussée Prince Louis Rwagasore 164, Bujumbura, Burundi.

^b Université Libre de Bruxelles, Département Aéro-Thermo-Mécanique (ATM), Avenue F.D. Roosevelt 50, CP 165/41, 1050 Bruxelles, Belgique

ARTICLE INFO

Article history:

Received 05 September 2022

Accepted 27 November 2022

Keywords:

Injector

Ansys workbench

Geometry

Mesh

Simulation

ABSTRACT

Cavitation is a physical phenomenon that often occurs in hydraulic machines such as pumps, valves, and turbines. Although the Banki-Michell turbine has been used for a long time in small hydropower, no study related to this phenomenon of cavitation in the injector of this turbine has been done. In this study, we will present the results of a numerical study carried out in the nozzle of a Banki-Michell turbine. The numerical solution of the Navier Stokes cavitation equations of the Banki-Michell turbine injector was carried out considering a 2D geometry of the injector-rotor assembly. The simulation results showed that the cavitation phenomenon appears when the water flow area in the nozzle becomes less than 50%. Furthermore, the results also showed that the occurrence of this cavitation phenomenon in the injector is more likely at higher operating heads. The results of an experimental study of the geometry of the injector showed that the height of the water passage section varies linearly with the degree of opening of the stator valve.

* Corresponding author, E-mail address: jean.bosco.niyonzima@edu.ub.bi

Tel.: +257 77759209

ISSN: 1112-2242 / EISSN: 2716-8247



This work is licensed under a Creative Commons Attribution-ShareAlike 4.0 International License. Based on a work at <http://revue.cder.dz>.

1. Introduction

The Banki Michell turbine is a crossflow turbine suitable for sites of heads lower than 200 m. The study made by Otsuka (2022) showed the presence of vibration in a Banki Michell turbine due to the pressure fluctuation by flow interference of the blade and casing wall [1]. Another phenomenon called cavitation is likely to limit the efficiency of this turbine. Some theoretical approaches show that the Banki Michell turbine is susceptible to the cavitation phenomenon when operating with partial flows [2].

Cavitation is a physical phenomenon that often occurs in hydraulic machines such as pumps, valves, and turbines. Cavitation is defined as a rupture of the continuous medium of the fluid due to geometrically imposed local overspeed, shear, acceleration, or vibration phenomena [3]. This results in a local pressure drop in the fluid. Cavitation is therefore the result of a local pressure drop below the corresponding saturation vapor pressure at a given liquid temperature. As illustrated in Table 1, the saturation vapor pressure of the water varies with local temperature [4].

A temperature of 20°C is associated with a saturation vapor pressure of water of the order of 2338.54 Pa.

Table 1. Table of vapor water saturation pressure [4]

Temperature (°C)	Pressure (Pa)	Temperature (°C)	Pressure (Pa)
20,0	2339	23,0	2810
20,5	2412	23,5	2896
21,0	2487	24,0	2985
21,5	2565	24,5	3076
22,0	2644	25,0	3169
22,5	2726		

The nozzle of a Banki-Michell turbine is the part that forms the inlet manifold converging towards the rotor on a rectangular passage section. The nozzle has a deflecting top wall whose curvature is appropriate to the angle of admission of the water lines to the turbine rotor. The injector is divided into two compartments, which gives it the ability to maintain the efficiency of the turbine when it is operating at flows below the nominal operating flow. Depending on the manufacturer, the injector can be divided into two equal parts or in the proportion 1/3: 2/3 [2]. Each compartment is then associated with a control valve whose main role is to vary the flow of water directed to the turbine wheel according to its availability upstream of the turbine. This technology allows the turbine to perform better even when operating at lower than nominal flow rates. However, the available literature shows that the type of vane is the source of the cavitation phenomenon. This is due to the reduction of the water flow area between the nozzle

body and the control valve seat. According to the continuity equation of the formula in Eq.(1) for all incompressible fluids, the volume ΔV of the fluid flowing through any cross-sectional area, as shown in Figure 1, remains constant for a time interval Δt [5]. This continuity equation shows that, for an incompressible fluid, the velocity of the fluid increases if the cross-sectional area of the pipe decreases.

$$\Delta V = A_1 v_1 \Delta t = A_2 v_2 \Delta t \quad (1)$$

According to the flow through a hydraulic pipe, the Bernoulli equation in any section of the pipe is given by the formula in Eq.(2). The sum of the pressure energy, kinetic energy, and potential energy is constant.

$$p + \frac{1}{2} \rho v^2 + \rho g z = \text{constante} \quad (2)$$

The static pressure p is equal to the ratio of force over a given section as shown by Eq (3).

$$p = \frac{F}{A} \quad (3)$$

Bernoulli's theorem as depicted by the Eq.(2) is valid when the used fluid is incompressible, in that case, each term of the equation constitutes an energy per unit volume [6]. A pressure density p due to the internal forces of the fluid, a kinetic energy density, and a potential energy density associated with gravity. As the flow rate remains constant despite the variation of the flow velocity, for continuity to be verified, the pressure must decrease [6]. Thus, when the velocity through a section of a pipe increases, the pressure decreases through that section. However, the cavitation phenomenon is most likely to occur through the smallest sections when the local pressure becomes lower than the saturating vapor pressure.

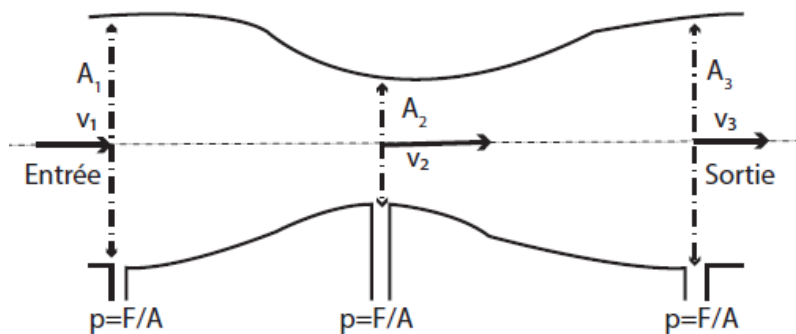


Fig. 1. Schematic diagram of the Venturi effect [6]

This numerical study aims to analyze, by numerical simulations of the flow, the phenomenon of cavitation likely to appear when there is a reduction in the cross-sectional area of the water flowing through the injector. The simulation tool used is the academic version of ANSYS

WORKBENCH. Workbench is a module of ANSYS applications working together to perform numerical calculations under FLUENT [7]. It consists of three software packages with well-defined purposes, namely Design Modeler, which consists of the creation or modification of the geometry of the simulation domain, Mesher, which is suitable for the realization of the mesh on the geometry, and Fluent, which is responsible for carrying out the calculations on the given mesh. The objective of this study is to present the results of a simulation study of the stator vane of the Banki-Michell turbine and on the other hand the results of experimental measurements of the water flow cross-section in the nozzle of this turbine. Apart from the introduction and conclusion, this study is developed in four parts. The first and second parts present respectively the theoretical background of the cavitation phenomenon and the CFD calculation methodology. The fourth part discusses the results of the simulations, while the fifth part presents the results of measurements carried out between the injector body and the control valve seat as a function of the opening degrees of the latter

2. Cavitation phenomena

2.1 Definition

According to Brennen (2011), cavitation is defined as the breakdown of the continuous medium of liquid under excessive stress [3]. Cavitation is therefore a physical phenomenon that affects liquids. Unlike boiling, cavitation is not due to an increase in temperature above the vaporization temperature but is due to a decrease in pressure below the vapor pressure for the local temperature conditions. As depicted in the Bernoulli equation (Eq.4), this low pressure is the consequence of a local increase in the flow velocity. This explains why Bernoulli's theorem is applicable to perfect fluids, stationary flows, and in the absence of heat transfer.

2.2 Dimensionless coefficient

In the study of the cavitation phenomenon, the used dimensionless parameter is sigma, σ , which is also called a cavitation number. This Thoma's coefficient is determined by model tests [8] and its value is given by the turbine manufacturer. In a hydraulic system susceptible to cavitation, as in the case of a hydraulic turbine, by defining p as the local pressure expressed in Pa, p_v as the water vaporization pressure in Pa, ρ as the density in kg/m³ and v as the flow velocity in m/s, the cavitation number calculated according to relation of the Eq (4) [3][9]. This relation expresses the ratio of the local pressure to the dynamic pressure at a point in the system.

$$\sigma = \frac{p-p_v}{\frac{1}{2}\rho v^2} \quad (4)$$

In the case of hydraulic turbines, the value of σ is defined according to the type of turbine. As an example, the cavitation number of the Francis turbine calculated through the Eq.(5) is the result of empirical studies and allows us to estimate the value of the cavitation number as a function of the specific speed N_{QE} of the turbine, the flow velocity V and the head H [4]. As shown by Eq (6), N_{QE} is the specific speed of the turbine calculated as a function of the flow rate and the hydraulic energy E . By defining an empirical value of the critical cavitation number, cavitation will be avoided in an installation if the value of the cavitation number is greater than the critical cavitation number [5].

$$\sigma = 1.2715 \cdot N_{QE}^{1.41} + \frac{V^2}{2gH} \quad (5)$$

This specific speed N_{QE} is defined according to the international standards IEC 60193 and 600041, and equation (6) shows that it depends on the rotational speed N (rpm), the volumetric flow Q (m³/s), and the hydraulic energy E (J/kg).

$$N_{QE} = \frac{NQ^{1/2}}{E^{3/4}} \quad (6)$$

2.3. Cavitation inside the Banki-Michell injector

According to Chérière (1986), the classical flow control device of a Banki-Michell turbine is a valve called an aileron valve. Although it has been widely proven to be efficient, this valve is subject to cavitation below 50% of its opening [2]. Indeed, a performance test of the JLA 29 turbine, which is a typical Banki Michell turbine, was carried out and the results showed that its efficiency can reach 80% when the valve is fully open [10]. In addition, engineers from JLA hydro, observed that the JLA 29 turbine presents a cavitation phenomenon when operating under a partial flow rate and with a head of more than 20 meters. Notice that JLA 29 turbine is a typical Banki-Michell turbine made by the JLA HYDRO Company.

Indeed, as depicted in Figure (2), the valve rotates through an angle of 26° from the closing and opening positions. The geometry of the injector was drawn using the SpaceClaim module. The module is one of the three modules of the Ansys Workbench. By moving the mobile valve under 50% of the opening, we can see that the cross-sectional area is decreasing significantly.

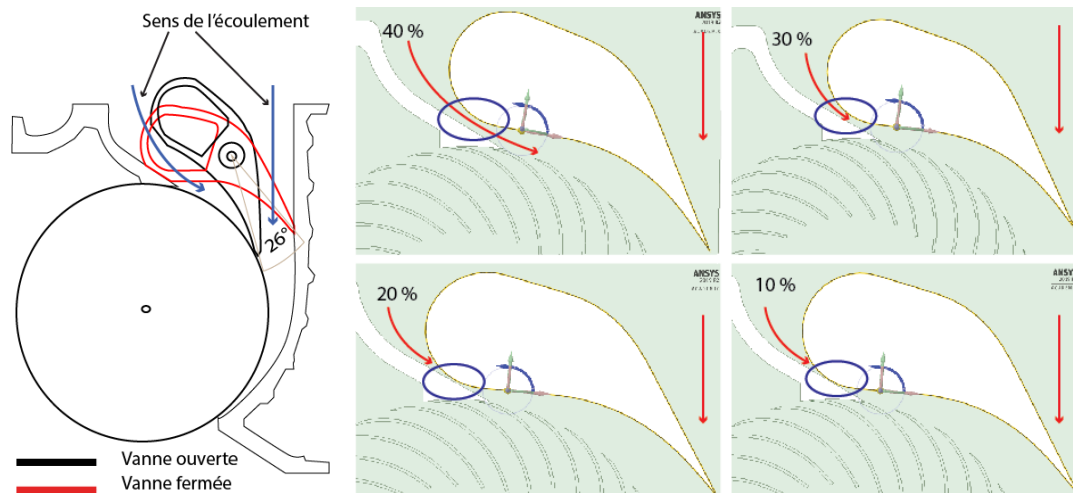


Fig. 2 (left) Profile of an open and closed valve, (right) Cross-section variation of the water

The study of the cavitation phenomenon is therefore logically concerned with the water flow cross-section in the injector, the cavitation zone located between the turbine injector walls, and the control valve body. The height of the water flow area changes depending on the opening position of the valve.

3. CFD calculation method

3.1 Navier-Stokes Equation

As illustrated in Figure 3, the formulation of the Navier-Stokes equation for a moving particle is achieved by determining the viscosity force due to the frictional forces exerted on an elementary volume. The calculation of the viscosity force is based on two assumptions: a Newtonian fluid and an elementary volume dV assumed to be incompressible [6].

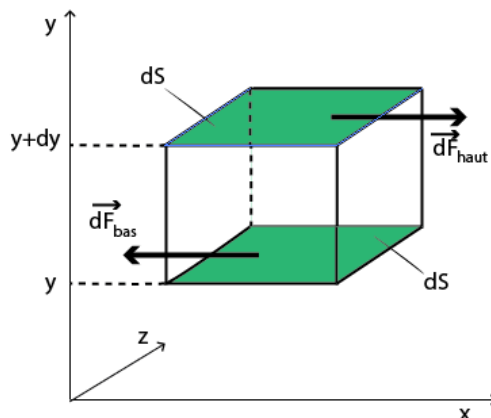


Fig. 3. Schematic illustration of viscosity forces on an elementary volume

As illustrated by Eq.(7), the viscosity force is equal to the difference between the surface forces applied on the two elementary surfaces dS_1 and dS_2 [6]. It is then calculated using the derivatives formula of Eq.(7).

$$dF = \left(\mu \frac{\partial v(y + dy, t)}{\partial t} - \mu \frac{\partial v(y, t)}{\partial t} \right) dS \cdot \bar{u}_x \quad (7)$$

Navier-Stokes equation is a writing of the fundamental principle of dynamics for a fluid particle subject to several forces such as gravity force, pressure forces, and viscosity force. As illustrated by Eq. (8), the product of the density and the acceleration of the fluid particle at point M in the flow is equal to the sum of its gravity, the pressure forces, and the viscosity force [6].

$$\rho \left(\frac{\partial \bar{u}}{\partial t} + (\bar{u} \cdot \text{grad}) \bar{u} \right) = -\text{grad}p + \rho \bar{g} + \mu \Delta \bar{u} \quad (8)$$

As shown in Figure 3, the velocity field at a point M at time t coincides with the velocity vector u of the fluid particle passing at time t through a point M in space. The fluid particle then acquires a so-called local acceleration noted $\partial \bar{u} / \partial t$ due to the simple temporal variation of the velocity at a given point. As the fluid particle is in motion, it does not have the same speed between two different points in space. It then acquires an acceleration due to its convection during the flow, noted $(\bar{u} \cdot \text{grad}) \bar{u}$. However, the complexity of the Navier-Stokes equation comes from the non-linearity of the momentum convection term which makes the equation non-linear, and the viscous diffusion term which introduces the second-order derivatives.

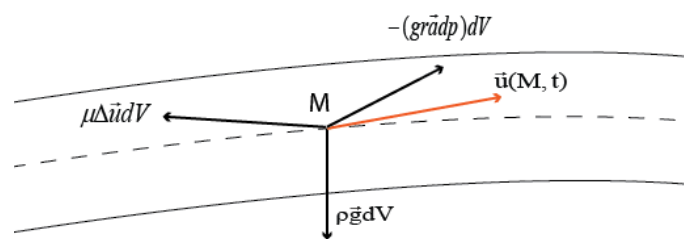


Fig. 4. Illustration of the N-S equation formulation

3.2 Geometry of the domain

As shown in Figure 5, in this simulation we took the injector space along with the control valve and rotor at the bottom with a cover to facilitate the determination of boundary conditions in the simulation. In addition, the simulations will be performed in two dimensions because the benefit of the flow is identical in each lateral section of the injector.

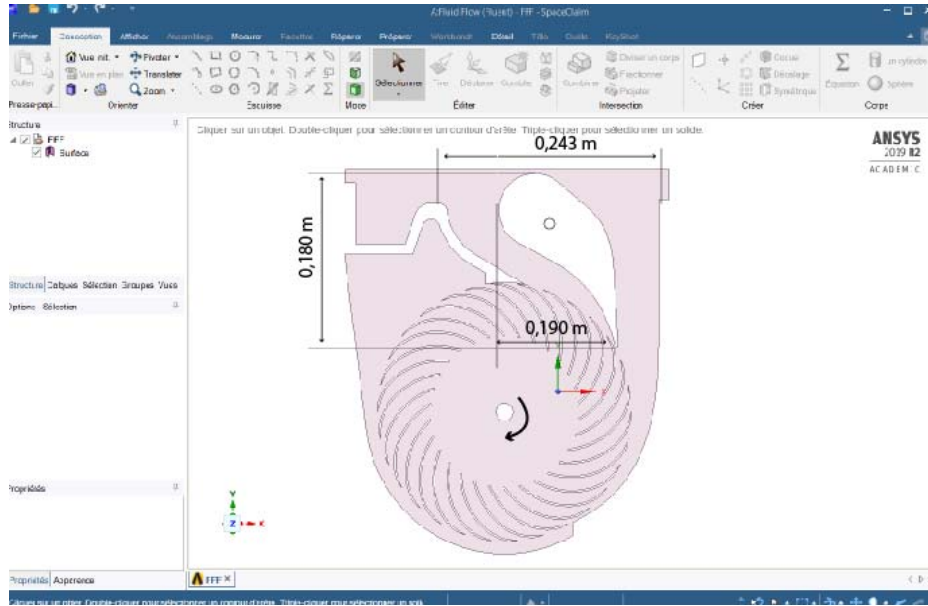


Fig. 5. Geometry domain

3.3 Mesh

To allow the discretization of the fluid mechanics' equations, we have meshed the injector with its valve and the turbine rotor. The mesh must indeed respect certain rules [11], such as: maintaining a good quality of the elements, ensuring a good resolution in the regions with strong gradients, ensuring good smoothing in the transition zones, and minimizing the total number of elements to have a reasonable calculation time. The resulting mesh is a single-face structured mesh for the injector and rotor. Figure 6 is an illustration of the mesh from the injector inlet to the rotor outlet. According to Eq.(9) [12], the height of the mesh is calculated as a function of the reference velocity around the valve, the length of the valve chord, the dimensionless height of the mesh y^+ , and the kinematic viscosity of the water ν (m^2/s). In this paper, we adopted a dimensionless mesh height y^+ between 30 and 300 [11] [13]. The interval [30, 300] is a valid range for a Fluent wall treatment [11]. The reference velocity at the inlet section is calculated according to Eq. (10) and is equal to 9.9 m/s. The absolute velocity depends on the acceleration of gravity g (m/s^2) and the nominal head h which equals 5 m in this case.

$$y = 6 \left(\frac{V_{ref}}{\nu} \right)^{-\frac{7}{8}} \left(\frac{L_{ref}}{2} \right)^{\frac{1}{8}} y^+ \quad (9)$$

$$V_{ref} = \sqrt{2gH} \quad (10)$$

The mesh was created using an academic version of the ANSYS Meshing tool, which can only support a mesh with several elements below 512,000. By replacing in formula (9) y^+ by 100 [11], we obtain a mesh height $y = 0.0005$ m. The mesh was therefore created with a mesh height

of 0.0005 m and the result of the meshing was some 489,769 elements. The computer used for the simulation is a laptop characterized by an i7-7700T -2.90 GHz processor and 16 GB RAM. As shown in Figure 6, the boundary layer is a zone where turbulent instabilities arise, where viscosity effects are important and where magnitude gradients are significant. It is important to refine the mesh in the vicinity of the solid walls to correctly capture the behavior in this boundary layer region [11].

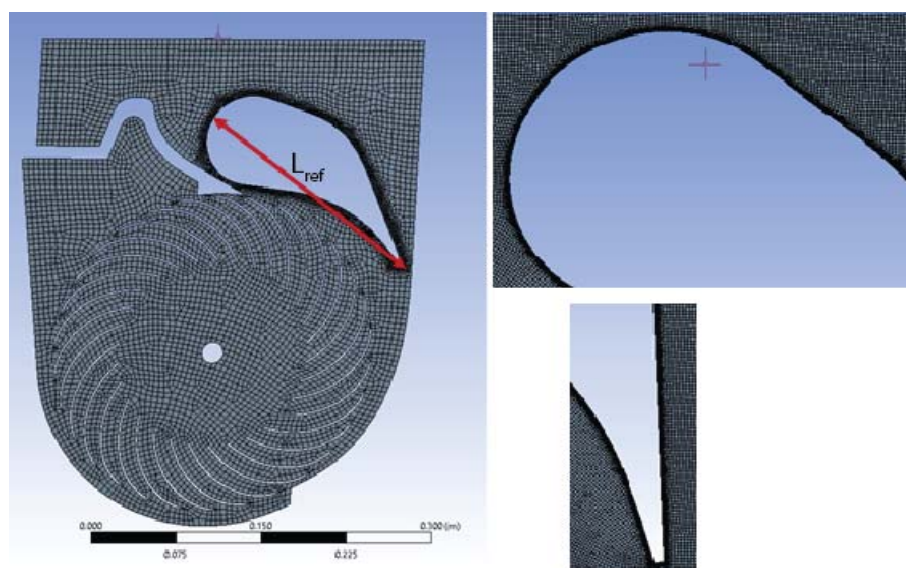


Fig. 6. Mesh

3.4 Boundary conditions

Several conditions are available, among which we distinguish between inlet, outlet, solid boundary conditions, etc. In this study, Fluent software was used to solve the equations and the Fluent interface offers the choice of inlet and outlet conditions [11].

- ✓ For the inlet: velocity inlet, pressure inlet, mass flow rate, etc.
- ✓ For output: pressure outlet, outflow, etc.

Indeed, the mass flow rate at the inlet of the injector is 195 kg/l and the pressure at the outlet of the rotor is said to be atmospheric [14]. The total pressure at the turbine inlet can therefore be calculated by applying Bernoulli's equation as illustrated by Eq.(11), in incompressible flow and neglecting the pressure drops. The pressure P is expressed in Pa, the velocity V in m/s, the density of water in kg/m^3 , the acceleration of gravity in m/s^2 , and the altitude Z in m. The subscripts 0 and 1 indicate the level of the upstream tank and the rotor inlet respectively. Figure 7 is an illustration used for the determination of the total pressure at the turbine inlet and the absolute total pressure at the rotor inlet is equal to the sum of the atmospheric pressure in the upstream reservoir and the pressure difference between the upstream level and the turbine axis as illustrated by Eq.(12). Knowing that the head is 5 m, the total calculated pressure is 150.4

kPa. These calculations have been made by neglecting the flow velocity in the upstream tank.

$$\frac{P_0}{\rho g} + \frac{V_0^2}{2g} + Z_0 = \frac{P_1}{\rho g} + \frac{V_1^2}{2g} + Z_1 \quad (11)$$

$$P_{tot} = P_o + \rho gH \quad (12)$$

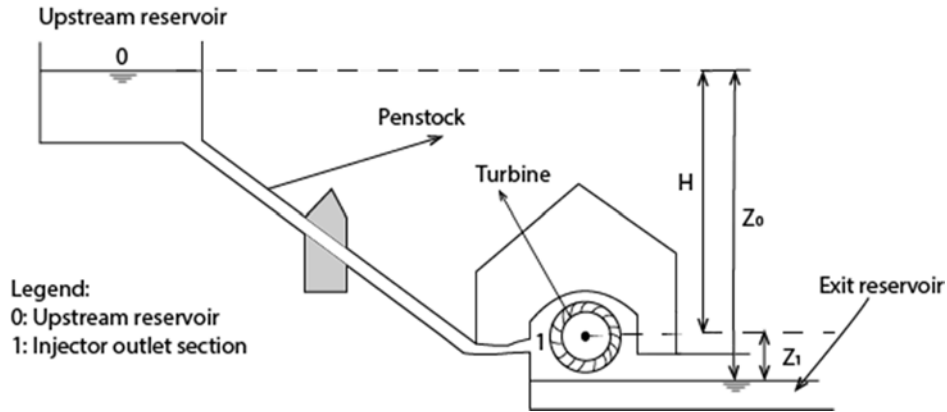


Fig. 7. Schematic principle of a Banki-Michell turbine [15][16]

On the other hand, as the turbine rotor is a rotating part, the setting of the boundary conditions must take into account the rotor speed. The rotational speed is expressed in rad/s. Since the turbine normally operates at a constant speed, the numerical simulation calculations were carried out using the nominal design speed of the turbine. The JLA 29 turbine operating at a head of 5 m is characterized by a rotational speed of 292 rpm or approximately 31 rad/s.

3.5 Solver parameters

For Fluent, two types of solvers are available: pressure-based and density-based. And since the fluid is incompressible, we used the pressure-based solver. Simulations were performed in the liquid phase and a steady state, so all flow quantities will remain constant as a function of time. The characteristic Reynolds number of the flow around the injector valve is defined according to the formula in Eq.(13) [6]. In this definition, the length L expressed in m represents the length of the valve chord, ρ being the density of water in kg/m^3 , u in m/s is the velocity around the valve and ν is the kinematic viscosity of the fluid in m^2/s .

For the JLA 29 turbine installed on the ATM laboratory test bench, the length of the valve chord is approximately 0.200 m.

$$Re = \frac{\rho Lu}{\mu} \quad (13)$$

$$Re = \frac{L_{ref} V_{ref}}{\nu} \quad (14)$$

In the case of this study, the Reynolds number is calculated as a function of the reference velocity equal to the velocity of the water around the injector valve, a reference length L_{ref} equal

to the length of the valve chord and the kinematic viscosity of the water ν . The Reynolds number calculated according to the formula in Eq.(14) is about 1.969.094 with a head of 5 m. As the Reynolds number is high, the turbulence of the flow must be taken into account. Fluent offers several turbulence models such as k-omega, k-epsilon, and Spalart-Allmaras. In the case of incompressible fluid flow as in this case study, the turbulence model used is typically the k- ϵ model [3][11]. This model is used for flows with a small pressure gradient.

4. Results and discussion

In this study, two sets of numerical simulations were carried out. The first set consisted of varying the opening level of the valve while maintaining the head of 5 m. This head corresponds to the nominal operating conditions of the JLA 29 turbine in the Banki-Michell turbine test bench installed at the hydraulic laboratory. This head corresponds to the nominal operating conditions of the JLA 29 turbine of the Banki-Michell turbine test bench installed at the ULB-ATM hydraulic laboratory. Simulations were carried out with a valve opening range of 30 to 100%. The ULB-ATM JLA 29 turbine does not operate stably at nozzle valve openings below 30%.

As illustrated in Figures 8 and 9, the small circle in red allows us to locate the water flow section in the turbine nozzle which constitutes the cavitation zone during the operation of the Banki-Michell turbine. The analysis of the results on the velocity field of the water in the cavitation zone shows that the increase of the flow velocity is inversely proportional to the level of the valve opening of the injector. As the cross-sectional width decreases, the flow velocity of the water in the cavitation zone increases. Figure 5.15 illustrating the velocity fields of the water in the cavitation zone, shows that the velocity reaches a very high value of 6.8 m/s for a minimum valve opening of 30%.

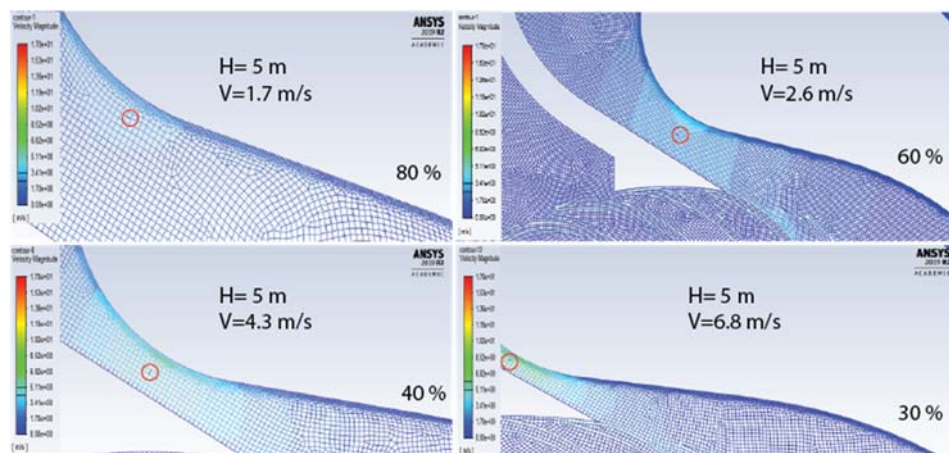


Fig. 8. Water flow velocities as a function of valve openings in %

In the case of the pressure fields of the flow, the local pressure of the fluid decreases more and more, proportionally to the position of the injector valve. The smaller the flow cross-section, the smaller the local pressure in the cavitation zone. Figure 9 shows the static pressure fields in the cavitation zone and the static pressure is 2,071.6 Pa for a valve opening of 30%.

The temperature measurements of the JLA 29 turbine test bench of the ULB-ATM hydraulic laboratory showed that the average temperature at the inlet and outlet of the impeller is 20°C. According to the climate table of the Jene area of Kabarore commune, the average daily temperature for the Jene area is also around 20°C. The Ryamukona site is located at the border of the Jene zone. For this case study, the cavitation phenomenon caused by the injector valve was defined by considering a saturating steam pressure value for a water temperature of 20°C. For this purpose, the operation of the JLA 29 turbine shows the cavitation phenomenon when the pressure in the cavitation zone becomes lower than the saturating steam pressure of 2,338.5 Pa, which is the case with a valve opening of 30%.

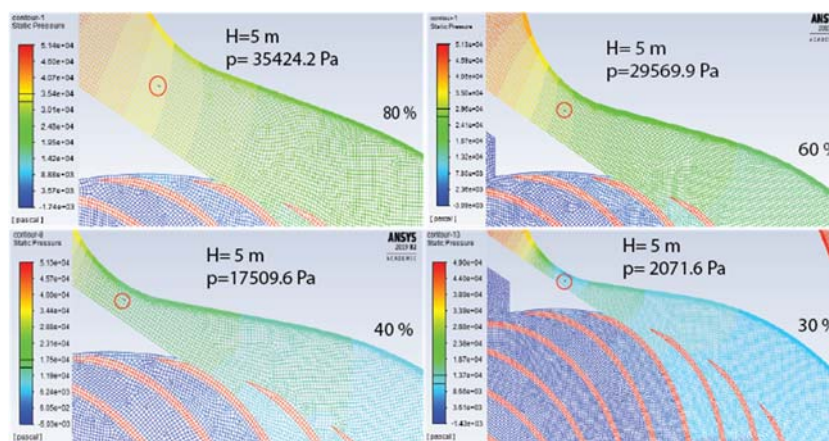


Fig. 9. Static pressure as a function of valve opening in %

Figures 10 and 11 show respectively a graphical representation of the evolution of the velocity and static pressure in the cavitation zone close to the aileron valve. The analysis of the results shows that the cavitation phenomenon appears during the operation of the JLA 29 turbine from an approximate opening of 30% of the injector valve. With 30% opening, the static pressure in the cavitation zone is of the order of 2,071.6 Pa, which is lower than the saturation vapor pressure of 2,338.5 Pa at 20°C water temperature [4]. The "critical" velocity of water is of the order of 6.8 m/s.

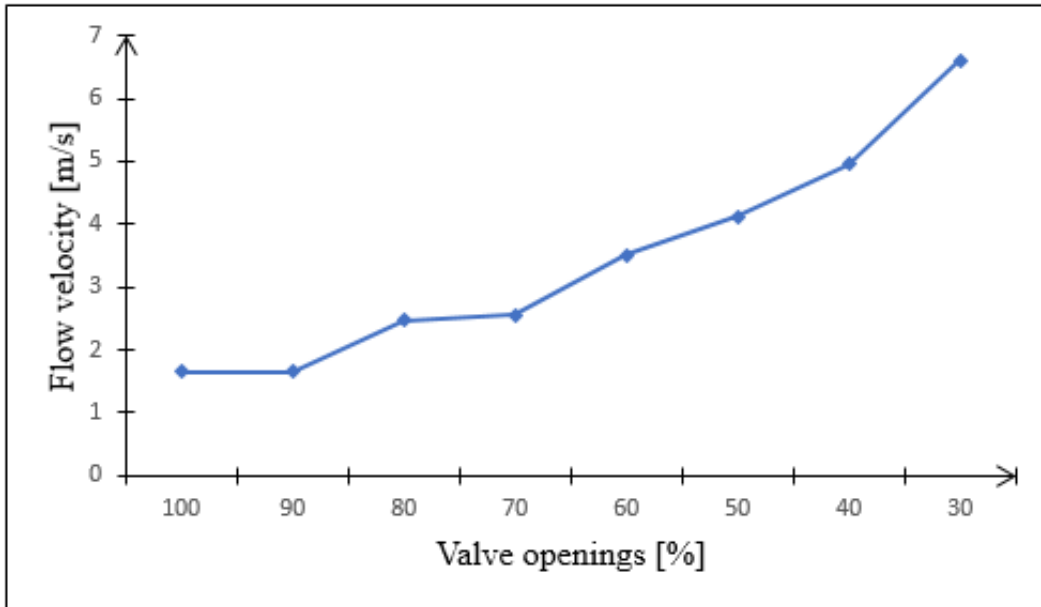


Fig. 10. Flow velocity in cavitation area for H=5.0 m

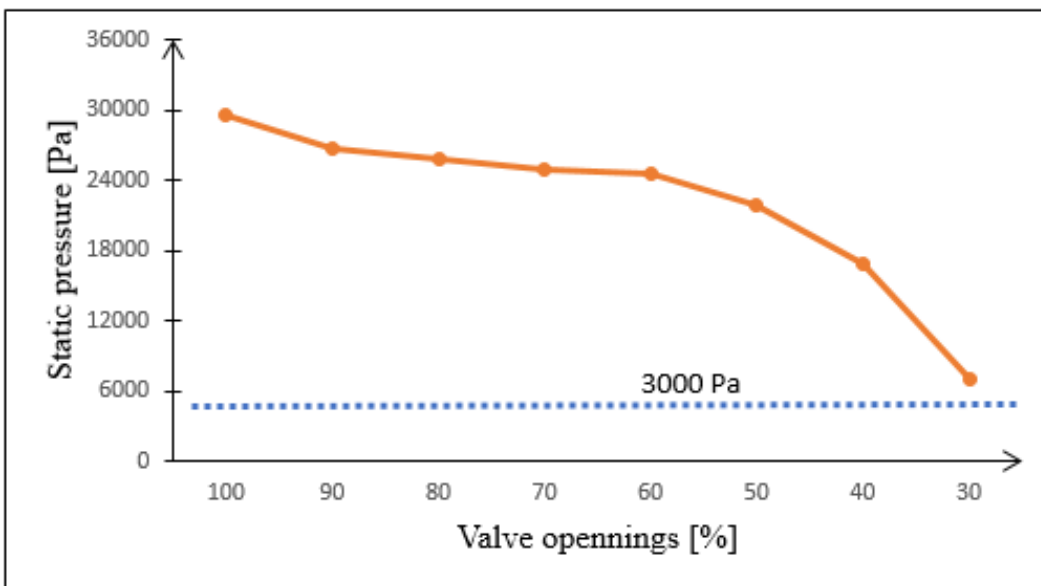


Fig. 11. Static pressure in cavitation area for H=5.0 m

To study the influence of the head on the occurrence of cavitation, another set of numerical simulations was carried out by varying, depending on the position of the valve, the head in the range of 5 m to 20 m. Figure 12 shows the static pressure results for a turbine operating at head $H = [5 \text{ m}, 6 \text{ m}, 7 \text{ m}, 8 \text{ m}]$ for a valve opening of 30%. It can be seen that the static pressure continues to drop in the cavitation zone until it reaches negative values.

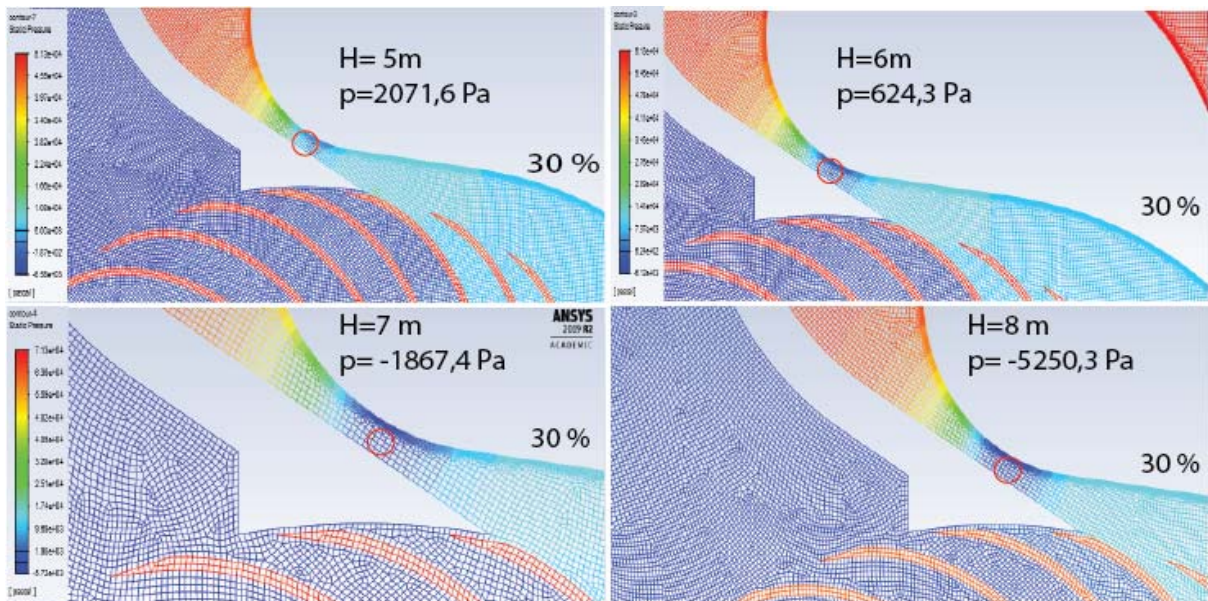


Fig. 12. Evolution of static pressure for H = [5 m, 6 m, 7 m, 8 m]

In the case of heads varying between 5 to 20 m, the evolution of velocities and static pressure in the cavitation zone are shown in Figures 13 and 14 respectively. The result is that the cavitation phenomenon appears earlier, i.e. when the opening of the nozzle valve becomes less than or equal to 40% and no longer 30%, for a turbine operating at H = 20 m. For the same 40% valve opening, the static pressure is 4.536 Pa for a turbine operating at a head H= 15 m (with a critical water velocity of 11.3 m/s). It can therefore be seen that with 40% valve opening, the turbine does not yet experience cavitation when operating at a head of 15 m. It can be seen that, with a 40% opening of the valve, the "critical" head is therefore slightly above 15 - 16 m. It should be mentioned that during all simulations, the average water temperature between the inlet and the outlet of the impeller remained at about 20°C.

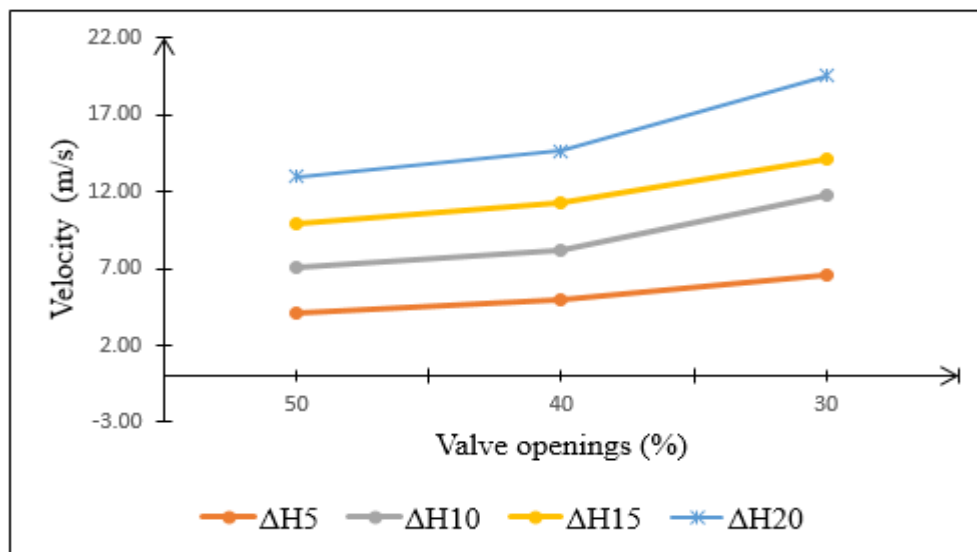


Fig. 13. Velocity field for different head operation

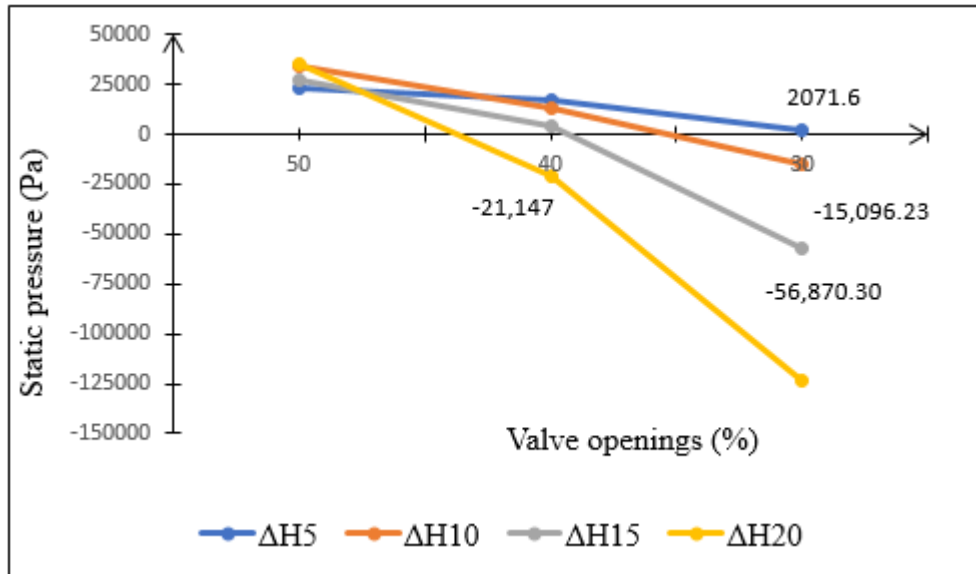


Fig. 14. Pressure field for different head operation

5. Flow cross-section measurements

From the results of the numerical simulations, it can be seen that the cavitation phenomenon appears when the cross-section of the water flow between the walls of the injector and the body of the control valve becomes smaller and smaller. To know the precise height of this section for the numerical simulations, an experimental study was carried out for this purpose using an IPLEX NX boroscope camera. Measurements of the height of the section were taken for each position of the valve. The variation of the valve position was done using a control system with an electric actuator driven by LabView 2017 software. The picture in Figure 5.22 shows a 2D and a 3D view taken by the boroscope camera during a measurement session. The results give a section height of 5.38 mm which corresponds to a 30% opening of the injector valve.

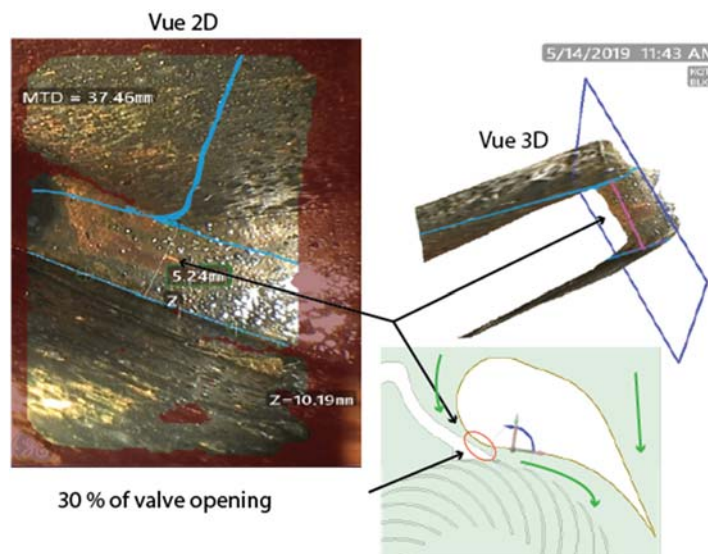


Fig. 15. A boroscope picture

The results of these measurements in Figure 16 show that the height of the cross-sectional area between the walls of the injector and the bottom of the control valve decreases quite linearly with the degree of opening of the valve. For a full opening of the valve, the measured height is 37 mm. The camera used takes measurements up to 20% valve opening. The smallest measurement made is a height of 1.38 mm obtained at 20% valve opening.

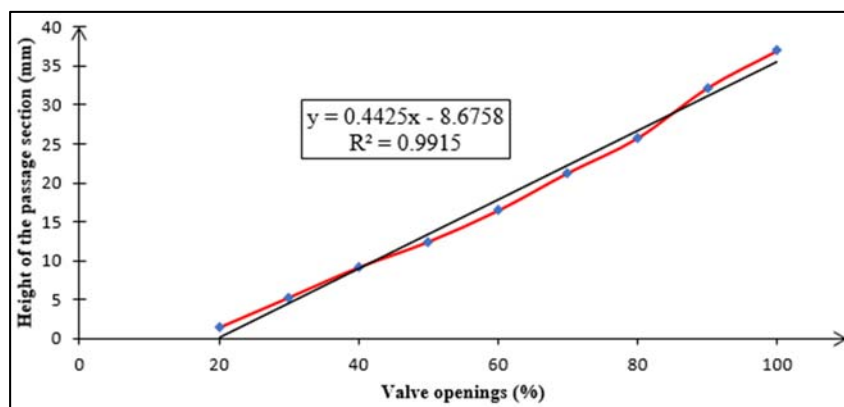


Fig. 16. Results measurements of a boroscope camera

6. Conclusion

The Banki-Michell turbine is a turbine with good efficiency over a wide range of flows throughout the year. Despite its good performance in terms of efficiency, the aileron valve fitted to the injector can be a source of cavitation when the turbine is operated at injector valve openings of less than 50% according to the literature.

The cross-sectional area of the water flow between the walls of the injector and the valve seat becomes smaller and smaller, which causes the local pressure to drop at this point. If the local pressure is lower than the vaporization pressure of the water, the water flow cross-section becomes the seat of the cavitation phenomenon.

With the JLA 29 turbine on the test bench installed at the ULB-ATM hydraulic laboratory, the study consisted of the numerical simulation of the flow in the injector using the Ansys-Workbench tool, under nominal operating conditions of the turbine, to monitor the evolution of the static pressure and water flow velocity fields in the potential cavitation zone. The results obtained show that, in this cavitation zone, the local pressures decrease more and more and the cavitation phenomenon appears at a valve opening position lower than or equal to 30%. In perspective, another numerical study is to be envisaged by cutting the foot of the mobile blade to improve the performance of the turbine with this blade.

7. References

- [1] K. Otsuka et al. "Characteristics and suppression of vibration in cross-flow turbine with a cavity." *Journal of Physics: Conference Series*. Vol. 2217. No. 1. IOP Publishing, 2022.
- [2] B. Chérière, "Création d'une gamme de turbines à flux traversant de turbines à flux traversant. *La Houille Blanche*, 1986, no 1-2, p. 55-62.
- [3] C. E. Brennen, "Invited Lecture An Introduction to Cavitation Fundamentals," no. July, pp. 1–17, 2011.
- [4] A. Wexler, "Vapor pressure formulation for water in range 0 to 100 Degrees C. A revision," no. 3, 1976.
- [5] E. Goncalves, "Modélisation et simulation de la cavitation," 2016.
- [6] O. Louisnard, *Cours de Mécanique des Fluides (Note du cours)*. Ecole des mines d'Albi, 2012.
- [7] K. L. Lawrence, *Ansys 10.0 Workbench tutorial*, Arlington: SDC Publications, 2006.
- [8] S. Colombo, "Abaque pour le calcul de la vitesse spécifique des turbines hydrauliques," *Houille Blanche*, no. 4, pp. 99–100, 1935.
- [9] European Small Hydropower Association (ESHA), *Petite Hydroelectricité. Guide technique pour la réalisation de projets*. Bruxelles: Maison des énergies renouvelables, 2005.
- [10] J.B. Niyonzima, "Lab performance testing of a small Banki-Michell hydraulic turbine for remote applications," *Journal of Renewable Energies*, vol. 24, pp. 244–260, 2021.
- [11] H. Nouri and F. Ravelet, "Introduction à la simulation numérique des écoulements. Application au transfert thermique sur plaque plane avec," 2012.
- [12] NUMECA International, "Flow Integrated Environment," p. 317, 2005.
- [13] J. B. Niyonzima, "Etude du potentiel hydroélectrique de la province Kayanza (Burundi): Application de la turbine Banki-Michell dans l'électrification des zones rurales," *Thèse de doctorat*, Université libre de Bruxelles, Ecole polytechnique de Bruxelles, p. 120, 2020.
- [14] A. Arter et U. Meier, *Harnessing WP on SM scale volume 2_Hydraulics-Engineering-Manual.pdf*. SKAT, Swiss Center for Appropriate technology, 1990.
- [15] A. Harvey et al., *Micro-Hydro Design Manual. A guide to small-scale water power schemes*, 1993.
- [16] J. B. Niyonzima and P. Hendrick, "Small Hydropower Development in Burundi," in *International Conference Sustainable Energy for Africa*, 2017, pp. 179–204.